Modelling and Predicting Land Use/Land Cover Dynamics in Semi-Arid Sudan Using Landsat Imagery, GIS Analysis, and the CA–Markov Chain Approach

AMNA. M.B. MARYOUD[1, a,*], AHMED. H. I. ElFAIG[2], RIHAB. M. M. ALSMANI[3], MOHAMED ENOUR. Y. AHMED[4]

[1] Department of Geography, Faculty of Education,
Alzaeim Al Azhari University– Khartoum,
SUDAN

[2] Department of Environment and Ecology,
Faculty of Geographical and Environmental Sciences, U of K, Khartoum,
SUDAN

[3] Department of Geography and Geographic Information Systems,
Faculty of Arts, Imam Abdulrahman Bin Faisal University, Dammam,
KSA

[4-]Department of Geography, Social Studies,
College of Arts, King Faisal University, Riyadh,
KSA

[a]https://orcid.org/0000-0002-1566-4016

**Corresponding author*

Abstract: - Land use and land cover change (LULCC) is a significant global issue, and projecting these changes is critical for informed policy decision-making. Understanding LULCC in semi-arid regions is essential for effective land management. This study aims to analyze past and future LULC in the semi-arid areas of Elkhuwei, West Kordofan, Sudan. We utilized Landsat images from 1980, 2000, 2010, and 2020 to assess historical LULC in the area. The results revealed that settlement and agricultural area in the study area increased, while bare ground decreased significantly between 1980 and 2020. The two periods exhibited different trends. Between 1980 and 2000, vegetation, settlement, and agricultural areas expanded, while bare ground decreased. Between 2000 and 2010 and 2010-2020, settlement and agricultural areas rose, while bare ground further declined. To predict land use and land cover changes (LULC) in 2030 and 2050, the Cellular Automata-Markov Chain model (CA-MC) was employed. The CA-MC model demonstrated improved results when assessing its application, indicating a trend toward increased population and deforestation. These findings contribute to developing effective land management policies and strategies to achieve or maintain sustainable development in the study area.

Key-Words: - land use and land cover, Detection, Prediction; GIS Techniques; CA–Markov Chain.

Received: August 11, 2025. Revised: November 17, 2025. Accepted: December 19, 2025. Published: February 16, 2026.

1 Introduction

Land use refers to the way a specific piece of land is utilized, such as for agriculture, wildlife habitat, parks, industry, or recreation. When these terms are used together, they typically refer to the classification of human activities and natural features on the landscape over a specific period, based on recognized scientific and statistical methods that utilize relevant source materials. Land-use/land cover (LULC) change has been ongoing throughout human history. [2], [10], [51]. Changes in global land use and land cover (LULC) are an important concern for future trends. Additionally, changes in LULC are vital for sustainability and managing natural resources. [49], [70], [63].

Land use and land cover change (LULC) present a significant challenge and a central focus of global change research. Land use, which refers to managing and modifying natural environments for various purposes, such as habitat and agriculture, differs from land cover, which encompasses the physical material at the earth's surface, including forests, wetlands, grasslands, and water bodies. These terms are often used interchangeably, despite their distinct meanings. [80], [28] estimates that around 420 million hectares of forest land globally are degraded, with 10 million hectares of forest cleared annually [33]. Since 1990, similar to the rest of the world, Africa has experienced significant changes in land properties due to the extent and intensity of natural resource extraction. [17], [35]. According to a report by FAO (2011), about 27.4% of Africa's land area (nearly 500 million hectares) is degraded. An extensive review of land use and land cover (LULC) in Africa found that

the expansion of agricultural land, driven by population growth, is the primary factor contributing to LULC changes, often at the expense of forested areas. [35].

These changes significantly impact essential components of our natural capital, including vegetation, water resources, and biodiversity. ([19], [1]. The dynamics of land use and land cover (LULC) change vary across different regions due to distinct driving factors. Many developed countries, including the United States, experienced significant deforestation driven by agricultural expansion and industrialization until the early 19th century. In contrast, urbanization dynamics and urban growth are often associated with demographic factors, particularly in developing countries. [13], [8], [31], [89].

Climate change, rising populations, the conversion of land use and land cover (LULC) into agricultural land, and the expansion of metropolitan regions have increasingly harmed various environmental processes, particularly ecological flow processes. These changes have resulted in the degradation of the overall functioning of the environment, diminishing the effectiveness of ecosystem services and hindering the full realization of the maximum benefits that can be derived from ecosystems [87], [20], [96]. Human activities have adverse effects on land use and land cover (LULC) in various regions worldwide. Changes in land use and land cover LULC induced by human actions are primarily driven by the needs of communities for food and economic development, which are exacerbated by the rapidly growing global population [6], [12], [16], [64]. Large-scale land use changes can fragment natural habitats, isolating species populations and disrupting ecological processes. Furthermore, land use and land cover (LULC) are often associated with either mitigating or the effects of natural hazards [28], [37]. In Sub-Saharan Africa, a dynamic LULC offers an inclusive sympathy of the interactions and relations crucial for sustainable land resource management [91]. The land use and land cover (LULC) compositions are undergoing rapid changes, particularly the conversion of forests to developed or urban settlements. These transformations are driven by increasing population growth, agricultural production, and other economic activities, which are essential for fostering growth and reducing poverty. [22], [84], [91], [3], [12, [16], [9], [21], [17].

In Africa, the expansion of agricultural land, driven by rapid population growth, has been identified as a primary factor influencing land use and land cover (LULC). The landscape has undergone significant changes due to the socio-economic and political transformations that took place in Europe during the first half of the 19th century. [76], [89], [16], [9], [12].

According to the United Nations (2019), 55% of the world's population, which amounts to approximately 7.8 billion individuals, currently resides in urban areas. This proportion is projected to increase to 68% by 2050. In Sub-Saharan Africa, 43% of the population lives in urban settlements. [85].

Land use and land cover in Sudan are influenced by a variety of factors, including the scale of the population, Land Tenure, and the nature of economic and social activities in the region, such as grazing, agriculture, the coal industry, and timber trade. Arable land in Sudan accounts for approximately one-third of the country's total area; however, only 21% of this arable land is actively cultivated. Additionally, over 40% of Sudan's total area is comprised of pastures and forests. [27]. Several researchers have examined changes in land use and land cover in Sudan [1], [4], [5], [25].

The techniques of remote sensing (RS) and geographic information systems (GIS) have proven to be powerful methods for evaluating the effects of climate change, particularly those related to land use and land cover (LULC). GIS and RS provide valuable approaches for understanding, analyzing, and monitoring LULC changes over time in various landscapes [83], [92], [97], [99], [100], [73]. Numerous studies on LULC have been conducted utilizing these tools. [8], [69], [64], [88], [79], [40], [77], [86], [18], [15], [48]. These models provide effective methods for detecting spatial variability patterns in land use and land cover (LULC). [88], [79]. Moreover, model validation is essential for accurately assessing land use and land cover (LULC) predictions in a specific area by comparing predicted changes with observed LULC changes. [30], [1], [64].

A CA-Markov model is a combination of cellular automata and transition probability matrices, generated by mapping between two different images. Markov chain analysis is a valuable tool for modelling land use and land cover change (LULC) when the changes and processes in the land use layer are difficult to describe. Additionally, the use of the CA-Markov model in LULC change studies offers several advantages, including dynamic simulation capabilities, high data efficiency, straightforward calibration, and the ability to simulate multiple land cover types and complex patterns. [68], [64]. The combined Cellular Automata (CA) and Markov Chain model (CA-Markov Model) is one widespread model used with high accuracy for analysing LULU dynamics [43], [42],[64],[24], [66]. Furthermore, the

CA-Markov model's robustness provides an opportune manner for modelling LULC change dynamics spatially and temporally in complex landscapes [38], [7], [94]. The flexibility of the CA-Markov hybrid model to integrate spatial and remote sensing data, along with biophysical and socio-economic information, facilitates a more comprehensive, detailed, and accurate projection of land use and land cover (LULC) change transitions. A critical aspect of the CA-Markov model is the transition rules, which are contingent upon the training data. [42], [13], [11]. The applied model is influenced by neighbourhood class and cell size, which are essential for achieving optimal simulation or prediction outcomes [34], [79]. CA-Markov hybrid model can effectively incorporate remotely sensed data and GIS. This model can convert the results into spatially explicit results necessary for LULC development [23], [34]. Some methods are based on the statistical matching approach for spatio-temporal data, utilizing key predictive variables [95]. Numerous studies have applied this model successfully in LULC prediction, e.g., [78], [43]. CA-Markov hybrid model used in this study is an effective and widely recognized method among researchers for detecting, predicting, monitoring, and simulating spatiotemporal changes in land use and land cover. (LULC). [15], [98], [54], [4], [29], [11], [80]. Recently, the detection and prediction of land use and land cover (LULC) changes have emerged as significant research topics in the field of remote sensing [98], [54]. Consequently, these issues have garnered the attention of numerous researchers and land use planners. [19]. Google Earth Engine (GEE) is an open-source, cloud-based geospatial processing platform that provides free access and open-source satellite datasets (Landsat, MODIS, Sentinel) with a high spatial resolution for extended periods. Google Earth Engine (GEE) is the most popular big geo data processing platform, which provides a set of state-of-the-art classifiers for pixel-based classification used for LULC mapping. The main advantage of GEE is the close link between the data and the algorithms, both of which are accessible via an Application Programming Interface (API) [93], [46], [75]. Advances in remote sensing and Geospatial Information Systems (GIS) have led to the development of high-resolution products for land use and land cover (LULC) models for mapping, detecting, and predicting changes in LULC. [54], [78], [88], [92].

In Sudan, several researchers dealing with LULC [40] and [4] argued that this change is primarily characterized by a decrease in forest and shrublands, alongside an increase in rain-fed agriculture and rangelands. The study observed degradation processes, particularly in vegetation cover, as a consequence of agricultural land expansion. It recommends the implementation of appropriate conservation and rehabilitation measures in forests and rangelands to mitigate the adverse effects of land degradation and desertification.

The changes were driven by human activity, underscoring the importance of effective land management practices and community involvement in mitigating Land Use Land Cover (LULC) changes. [5], [88], [41], [82]. Consequently, the impact of climate on land cover transformation has complicated the understanding of human-induced causes and can be observed and measured across various timescales. ([2], [73].

Land Use Land Cover (LULC) maps of a region offer valuable insights that help users comprehend the current landscape. Annual Land Use Land Cover (LULC) data from national spatial databases will facilitate the monitoring of temporal dynamics in agricultural ecosystems, forest conversions, surface water bodies, and other changes every year. Monitoring and mitigating the adverse effects of land use and land cover (LULC) dynamics while ensuring the sustainable generation of essential resources has become a primary focus for researchers and policymakers worldwide. LULC encompasses the various physical land types, including forests, wetlands, impervious surfaces, agricultural areas, and water bodies, as well as how humans utilize these land types within a given region[19], [44], [76], [36]. Assessment of land use change at different spatial scales is necessary from many perspectives, including sustainable development. [46], conservation and management of resources, land use planning [46], humanitarian programs, climate change impact assessment, and modelling.

2. Materials and Methods

2.1. Study Area

Elkhuwei is located within the west Kordofan State between latitudes 12°70′ and 13°84′ N and longitudes 28°42′ to 29°53′ E. Elkhuwei covers an area of 7956km^2. It has borders with four localities (Sheikan, Bara, Abuzabad, and En Nuhud) as shown in Figure 1. Elkhuwei is located within the semi-arid zone, where the longitudinal dunes are striking geographic landmarks. Climatologically, Elkhuwei has a rainy season from June to September, with an average annual rainfall of 450 mm. The yearly average temperature is approximately 30.04ºC. [81], [39]. The. Cultivated land is the major LULC class and accounts for more than 85% of the study area; the

remaining area is covered with grassland, shrubland, forests, and settlements. In the study area, rapid transitions of grassland, shrubland, and forest to cropland have been observed in recent decades. The majority of the area is dominated by rural agro-pastoral with scattered settlements and their livelihood is based on a mixed farming system by growing crops In addition, the potential for growth in different sectors, such as, livestock, and cultivation The study was selected because it is prone to soil erosion and environmental degradation as a result of intensive agricultural cultivation and overgrazing, as shown in previous studies.

Fig1. Map of the study area

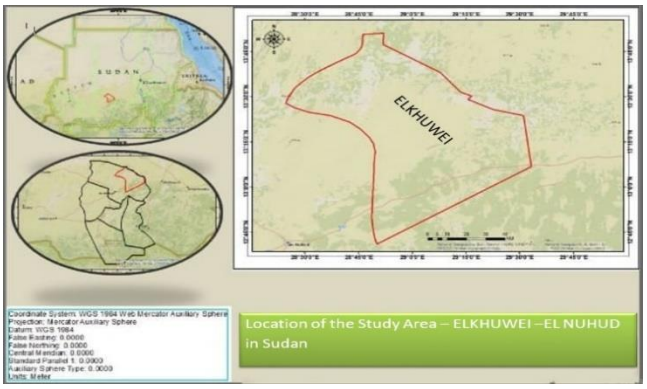

2.2. Data Types and Sources:-

The important spatial data required for the study were Digital Elevation Model (DEM), Landsat Images, and field data. The four Landsat images used were downloaded from the USGS, and DEM was obtained from the UNDP. The collected 10 m spatial resolution of DEM was used to develop the elevation and generate the slope of the study area. The analysis used the Landsat **1 MSS** from 1980, Landsat **4 TM** from 2000, Landsat **7 ETM+** from 2010, and Landsat **8 OLI 2** from 2020. The images were acquired in September (Table 1). The global positioning system (GPS) measurements were taken during fieldwork to verify and confirm the information gathered through remote sensing at each ground control point (GCP). The LULC types were noted for reference purposes.
Figure 2. False colour composites (NIR, red, and green bands) of (a)Landsat-1/MSS, (b)Landsat-4/TM, (c)Landsat-7/ETM+, and (d)Landsat-8/OLI 2 images used for LULC classification for the years (a) 1980, (b) 2000, (c) 2010, and (d) 2020. The deep red areas represent areas covered with shrubland; the darker red areas represent dense grassland, and the green areas represent agricultural land.

Table 1. Description of Landsat surface reflectance images used for LULC classification of the ELKhuwei Locality

Satellite	Satellite Sensor	Acquisition Date	User Bands	Total Bands	Spatial Resolution
Image 1980	1 MSS	Sep-21	1.2.3.4.5.7	7	30
Image 2000	4 TM	Sep-21	1.2.3.4.5.7	7	30
Image 2010	7 ETM+	Sep-21	1.2.3.4.5.7	8	30
Image 2020	8 OLI 2	Sep-21	1.2.3.4.5.7	9	30

Accordingly, the years 1980, 2000, 2010, and 2020, respectively. A table showing the number of training and testing/validation points collected for each LULC class can be found in the study area. For classification, the shape files of the collected training/testing data were imported as assets into the GEE environment. Furthermore, other LULC change driving variables, such as elevation, slope, distance from roads, and distance from towns, were collected from different sources and processed using ArcGIS Pro 3.0. The distance from roads was derived from the shape file of road network data acquired from the Open Street Map database. The distance from streets and the distance from towns were derived from the shape files of the stream network and town location, respectively. The elevation and slope were derived from the 10 m resolution DEM

2.3. Overview of the Methodology

This study mainly concentrates on LULC classification change detection and LULC prediction. The first part of the paper focused on LULC classification for the years 1980, 2000, 2010, and 2020 and change detection (1980–2000, 2000–2010, 2010–2020, and 1980–2020). Hence, satellite image collection, filtering image collection, computation of the median composite of filtered image collection, preparation of input variables, collection, and merging of training points, sampling region by integrating the median composite and merged training points, classification using the RF algorithm, accuracy assessment, and exporting of classified images were performed in the GEE (Google Earth

Engine). LULC images and change detection were performed using ArcGIS Pro 3.0. (Figure 3).

Figure 2 Landsat Images for Years 1980, 2000, 2010, and 2020

a 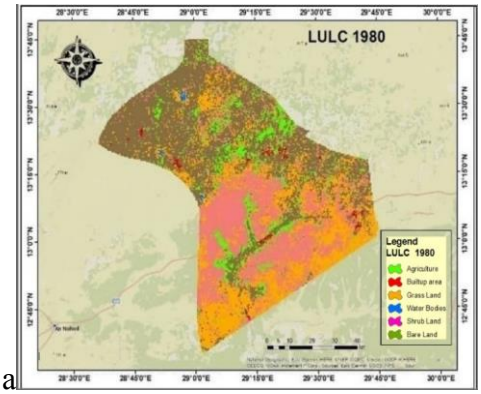

b 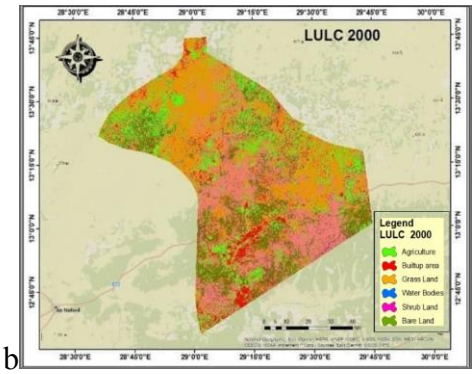

c 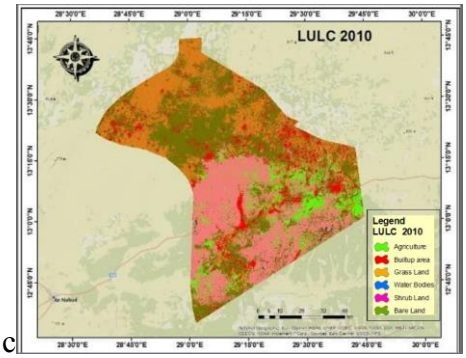

d 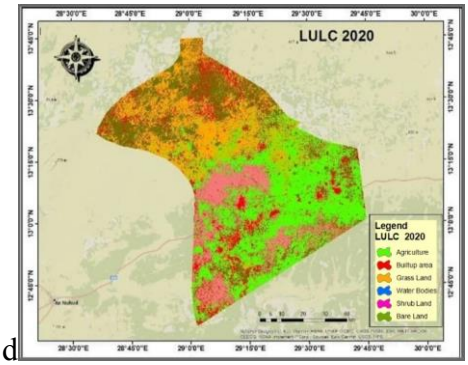

Figure 3. The methodological framework of LULC classification and change detection.

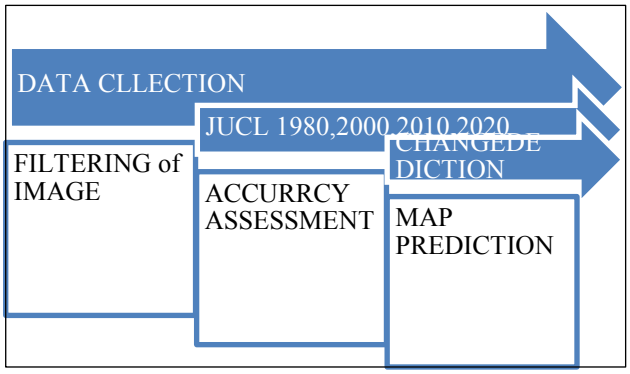

For LULC predictions, as presented in Figure 3, for the years 2030 and 2050, the images classified from LULC change driver variables processed in ArcGIS Pro 3.0 were used as inputs for the LULC prediction model. The CA–Markov model was used for the prediction. The procedures of this section were as follows:

- Preparation of input data (historical classified images and LULC change driver variables);
- Computation of transition probability matrices using the Markov model;
- Calculation of transition suitability maps;
- Prediction of LULC maps using the CA–Markov model for the reference year (2020);
- Validation of the CA–Markov model using the predicted and reference map of the year (2020); and
- Prediction of future LULC under the Elkhuwei and scenarios for 2030 and 2050. This study selected LULC prediction years (2030 and 2050) to examine the land use dynamics of the study area.

2-3-1-Pre-processing and classification

Pre-processing satellite images is essential to prevent data distortion or manipulation and to establish a direct connection between the data and biophysical phenomena. We employed atmospheric and topographic correction procedures in ERDAS Imagine to eliminate haze, atmospheric noise, and surface reflectance that may result from the Earth's rotation. A key function of pre-processing is to account for the movements of acquisition systems and platforms, particularly when using optical sensor data. Atmospheric correction specifically targets the removal of haze primarily caused by water vapour, fog, dust, smoke, or other particles in the atmosphere [56].

2.3.2. Post-processing

After pre-processing the satellite images, supervised classification was performed using the Maximum Likelihood Classification (MLC) technique to generate image classifications. The MLC method is a widely used algorithm for supervised satellite image classification. [21], [56]. The method has a strong theoretical foundation and can accommodate varying data, LULC types, and satellite systems [21]. After the preparation of the classification, one of the most widely used image classification techniques, i.e., maximum likelihood classification adapted for mapping all the land use and cover classes. Before selecting training samples, an empirical analysis of satellite imagery, Google Earth images, and a toposheet of the watershed was conducted carefully.

2.3.3. Land use and Land-cover classification

The number of LULC classes is preferred based on the requirements of a specific project for a particular application. Five major LULC classes were chosen for mapping the study area: agricultural land, bare land, built-up land, forest, and water bodies (Table 2).

Table 2. Classification of LULC in the Elkhuwei

LULC Class	Description
Shrub land	Areas of land covered with open and closed bushes and shrubs are mainly found along the wadis.
Grassland	Areas covered with grasslands are mainly used for grazing.
Agriculture land	Areas of agricultural land are mainly used for crop cultivation.
Bare land	Areas devoid of vegetation, e.g., sediments, exposed rocks, landslide zones, and degraded forest area
Built-up	Areas of urban and rural settlements and other developments like roads.
Water Body	Areas covered by wadi and reservoirs

2.3.4. Classification Accuracy Assessment

Foody et.al (2020) argued that assessing the classification accuracy provides confidence in the results and the subsequent change detection. In this Study, for 1980, 2000, 2010, and 2020, the reference points were collected from Google Earth, original Landsat images, previous reports, and maps. The common and most effective method used to measure the accuracy of the classified image from remotely sensed imagery is an error/confusion matrix [93], [14]. The confusion matrix provides overall accuracy, user accuracy, producer accuracy, and kappa statistics. Kappa coefficient was determined by using Equation (1). A kappa coefficient value below 0.0 shows poor agreement, a value between 0.41 and 0.60 depicts moderate agreement, and a value greater than 0.80 shows strong agreement. The Kappa coefficient is widely used in LULC assessments for accuracy to measure the true agreement between the observed agreement and chance agreement [93].

The Kappa coefficient is calculated by

Kappa

$$\mathcal{K} = \frac{\mathrm{P}o - \mathrm{P}e}{1 - \mathrm{P}e} \quad \textbf{(1)}$$

Where

po is the proportion of observed agreements, and

pe is the proportion of agreements expected by chance, Equation (2 and 3 respectively).

$$\mathcal{P}o = \frac{1}{\mathrm{N}}\sum_{i=1}^{\mathrm{N}} n_i \quad \textbf{(2)}$$

Where

N is the total number of observations or categories

n_i is the value (often a count or score) for the i-th observation.

$$\mathcal{P}e = \frac{1}{\mathrm{N}^2}\sum_{\mathrm{i}} n_{\mathrm{i}} + n_{+\mathrm{i}} \quad \textbf{(3)}$$

Where

N is the total number of observations (total in the table).

$n_{\mathrm{i}} +$ is the row total for category i (sum across columns in row i).

$n_{+\mathrm{i}}$ is the column total for category i (sum down rows in column i).

In agreement statistics (e.g., kappa), this Pe represents the expected proportion of agreement by chance, computed from the row and column marginal totals.

The contingency table is a matrix form that illustrates the frequency distribution of the variables and is used to show the interrelation between cells in this study. The interaction of every cell is tabulated into a matrix and calculated. The result explains the agreement of every criterion of each cell. Finally, the contingency table expresses the percent agreement as a Kappa coefficient. [93].

Kappa coefficient

$$\mathcal{K} = \frac{\mathrm{P}\mathrm{o} - \mathrm{P}e}{1 - \mathrm{P}e}$$

(4)

2.3.4. Land Use Land Cover Change Drivers

LULC change simulation studies have used topographic and distance driver variables. Elevation, slope, distance from roads, distance from streams, distance from urban areas, and evidence likelihood Rasters were considered potential driver variables. Distance from roads, distance from streams, and distance from urban areas were set as dynamic variables to express the varying distances as they change over time [90], [50], [58], [31].

2.4. LULC Change Prediction and Validation

2.4.1. LULC Prediction

The trend variations of LULC changes for the years 1980, 2000, 2010, and 2020 were analyzed to predict future years of the study area. The future land use scenarios were based on recent trends, historical land use information, and anticipated future change

2.4.1.1. Markov Model

A Markov model is a mathematical framework used to describe a sequence of events in which the probability of each event depends solely on the state of the preceding event. This characteristic, known as Markov models, has extensive applications across various fields, including data analysis, forecasting, and environmental modelling ([23].

Markov Model Formula

To predict future states, we use the following formula:

$$\mathrm{S}(\mathrm{t}+1) = \mathcal{S}(\mathrm{t})P$$

(5)

Where:

- St: is the state vector at time t (i.e., the distribution of future states).
- St−1: is the state vector at the previous time.
- P is the transition matrix that represents the probabilities of transitioning between different states.
- **State Vector:**
  $S(t) = [_{s1}(t), _{s2}(t), \ldots, _{sn}(t)]$

(6)

Where:

- S(t)= configuration of the entire system at time t
- n = total number of cells
- si(t) = state of cell i at time t
- si(t)∈S (finite set of states, e.g. {0,1})

Transition Probability Matrix:

$$\rho_{ij} = \frac{\mathrm{N}_{ij}}{\sum_i \mathrm{N}_{ij}} \qquad \sum_{\mathrm{j}} \rho_{ij=1}$$

(7)

Where

- ρ_{ij} = probability that a cell transitions from state i → state j
- N_{ij} = number of observed transitions from state i to state j
- $\sum_i \mathrm{N}_{ij}$= total transitions **out of state** i

This guarantees that probabilities are valid:

$0 \leq \rho_{ij} \leq 1$ and $\sum_{\mathrm{j}} \rho_{ij=1}$

Markov Chain Analysis is often employed to simulate complex systems. Processes such as land-use change are primarily used to examine the transition probabilities between different states. An initial state and a final state are used to determine the transition trends among different land uses. Markov chain analysis is a discrete random process that operates in both time and state.

The CA-Markov model is a hybrid of Cellular Automata (CA) and Markov Chain analysis. It is widely utilized in predicting and modelling land use and land cover change (LUCC). This integrated approach combines the spatial dynamics of CA with the temporal transition probabilities of Markov Chains, making it a robust tool for simulating and forecasting land use changes over time. [72].

2.4.1.2. The CA–Markov Model

Cellular Automata (CA) is a powerful modelling approach for simulating spatial and temporal dynamics in complex systems, including land use and land cover changes. CA models consist of a grid of cells, each with its state, and evolve based on simple rules that govern how the state of each cell changes. These models are beneficial for simulating systems where local interactions between neighbouring cells lead to emergent global patterns. [72].

The weight factor is combined with the transition probabilities to predict the state of adjacent grid cells, ensuring that land-use change is not a completely random process. The commonly used neighbourhoods are Moore, extended Moore, and von Neumann. In this study, we used the von Neumann neighbourhood.

The rules are suitability maps that indicate the likelihood of a cell transitioning from one state to another.
The model expression is:

$$S_i^{(t+1)} = f(Se^t, N_i^t, P) \quad \textbf{(8)}$$

Where:

- S_i^{t+1}: The state of cell i at the next time step t+1.
- S_i^t: The current state of cell i at time step t.
- N_i^t: The states of the neighbouring cells of i at time step t.
- F: The transition function that determines how the cell's state evolves based on its current state and the states of its neighbours.
- P: A set of parameters (such as transition probabilities, environmental constraints, or socio-economic factors) that influence the state change.

  Suitability maps $Sj(x)$are derived from standardized driver variables (e.g., distance to roads, slope, settlement proximity), each normalized to [0, 1].

$$Sj(x) = \sum_k w_k \ f_{k,j}(x) \quad \textbf{(9)}$$

Where:

- $f_{k,j}(x)$ = standardized driver variable (k)
- $w_{k=}$ = weight assigned to driver (k)
- $\sum_k w_{k=} \ 1$

2.4.2. Model Validation

Validation is simply a procedure to assess the quality of the predicted LULC map against a reference map. The images of Landsat for 1980, 2000, 2010, and 2020 were utilized to simulate the 2030 LULC image. The comparison of the simulated LULC image with the actual map was developed. The LULC of the years 1980, 2000, 2010, and 2020 were provided to calibrate Ac Markov, and the model was validated by simulating the recent LULC map of 2020. The validation process in AC Markov involves a cross-tabulation in a three-way comparison between the later land cover map (1980, 2000, 2010 the predicted land cover map (2030 and 2050), and the actual map (2020). The module validation in the ACM model was used to statistically evaluate the quality of the predicted 2030 and 2050 LULC images against the reference images [70]. The map shows areas where the model correctly predicted, called "hits", areas where the model predicted a change but it did not occur, called "false alarms, and occasions where the model was unable to predict it, but areas were changed in reality, called "misses". After the model prediction capacity was verified between the 1980 and 2000 time periods for 2020, the simulation process was repeated to project the 2030 and 2050 maps using the 2010 and 2020 classified maps. The other method is the kappa coefficient calculation between the predicted map and the actual land use map. However, the original kappa coefficient does not distinguish between the quantification and location error, delimiting its expressiveness. This can be resolved by calculating cause-dependent K-indices, Kno (kappa for no information), Klocation (kappa for location), Kstandard (kappa for standard), and KlocationStrata (kappa for stratum-level location) [53]. The overall agreement of the projected and reference map indicates the Kappa for no information (Kno). The location kappa (Klocation) is used to compute the spatial accuracy in the overall landscape, because of the correct assignment values in each category between the simulated and reference map [59]. The ratio of inaccurate allocations by chance to the correct assignments is kappa for standard (Kstandard). The kappa for stratum level location (Klocation Strata) is a quantification of the spatial accuracy within pre-identified strata, and it indicates how well the grid cells are situated within the strata. The blend of Kstandard, Kno, Klocation, and Klocation strata scores are considered for a comprehensive evaluation of the overall accuracy in terms of location and quantity (Table3). Additionally, the statistics considered are agreement quantity, agreement chance, agreement grid cell, disagreement grid cell, and disagreement quantity, which are used to know exactly how strong the agreement is between the simulated map and the base map (Table 4) [94].
The Disagreement Quantity and Disagreement Grid Cell constituents are crucial to understanding the simulated model. This validation method gives an idea about the level of agreement or disagreement between projected and actual LULC maps (Mas et al. 2012). The two most important differences between the two categorical maps are in terms of quantity (changes or persistence) and allocation. Disagreement by quantity is the variation between two images because of an imperfect combination in the overall proportions of LULC categories. The allocation disagreement is the distinction between two images caused by an imperfect combination among the spatial allocations of all land cover map categories [94].

Classification agreement/disagreement

Table 3: According to the ability to specify accurately quantity and allocation

Information of Allocation	No[n]	Medium[m]	Perfect[p]
Perfect[P(x)]	P(n) = 0.2146	P(m) = 0.9327	P(p) = 1.0000
PerfectStratum[K(x)]	K(n) = 0.1473	K(m) = 0.9327	K(p) = 0.9327
MediumGrid[M(x)]	M(n) = 0.1473	M(m) = 0.9327	M(p) = 0.9327
MediumStratum[H(x)]	H(n) = 0.1429	H(m) = 0.8620	H(p) = 0.8631
No[N(x)]	N(n) = 0.1429	N(m) = 0.8620	N(p) = 0.8631

Table 4. Possible ranges of map comparison and level of agreement of kappa values

No	Values	Strength of Agreement
1	<0	Poor
2	0.01–0.40	Slight
3	0.41–0.60	Moderate
4	0.61–0.80	Substantial
5	0.81–1.00	Almost Perfect

2.5. Land Use Land Cover Change Analysis

The CA Markov determines how the factors influence future LULC change, how much land cover change took place between earlier and later LULC, and then calculates a relative amount of transitions [93]. The future land use scenarios were based on recent trends, historical land use information, and anticipated future changes. The CA Markov uses the "change analysis" tab, the "transition potentials" tab, and the "change prediction" tab. The change rates were determined through the "change analysis" tab, along with the "transition potential" maps to simulate the future scenario [55].

The LULC dynamics in each study period were assessed using numerical values extracted from the classified images. To acquire the change pattern, the classified images from consecutive periods were cross-tabulated and compared with each other. The probability matrix was created between 1980 and 2000, 2010 and 2020, 2020 and 2030, and 2030 and 2050 using CA Markov. The change percentage [55] and the rate of change were determined for LULC categories using Equations (7) and (8), respectively, to establish the number of changes experienced among the different LULC categories during these periods.

Percent of change =

$$\%\nabla X = \frac{Xt_2 - Xt_1}{Xt_1} \times 100\%$$

Unit is percentage (%) and $Xt_1 \neq 0$.

(10)

Rate of change (km/year) =

$$\nabla X = X\_t2 - X\_t1$$

(11)

Where

- ∇X Amount of change in variable X
- Xt_1 Value (or state) of X at initial time t1
- Xt_2 Value (or state) of X at later time t2

3. Results and Discussion

3.1. Classification Accuracy Results

3.1.1 Accuracy Assessment of the Classified Images

The evaluation of accuracy for land use and land cover (LULC) change analysis was conducted by generating a confusion/error matrix for each LULC category across the classified maps of 1980, 2000, 2010, and 2020. The assessment utilized overall accuracy, kappa statistics, as well as producers' and users' accuracy. The kappa statistics and overall accuracy for the classified images were recorded as 82.9%, 79.3%, 89%, and 86.1% for the years 1980, 2000, 2010, and 2020, respectively (see Table 5).

The accuracy results for the more recent LULC maps were notably higher, which may be attributed to the enhanced spatial resolution of the satellite imagery. An accurate assessment of LULC is essential in any study employing remote sensing Landsat data for historical LULC analysis.

3.2. Analysis of Land Use and Land Cover Types

The analysis of Land Use and Land Cover (LULC) was conducted through the assessment of gains, net changes, and losses experienced by various categories, utilizing change analysis within the CA Markov framework. Spatial and temporal changes among different classes were evaluated for the years 1980, 2000, 2010, and 2020, as illustrated in Table 8. The transformations categorized are summarized in

terms of loss, gain, and net change of LULC, as depicted in Figure 4. The area coverage of LULC classes, their percentage, and the rate of change in the study area between 1980, 2000, 210, and 2020 were quantified and analysed in Table 6.

The gain in LULC for each class was determined based on the results of persistence and the total column value, while the loss was derived from the total row, with persistence also being calculated from the total row.

Table 5. Accuracy assessment of classified LULC maps for 1980, 2000, 2010, and 2020.

LULC 1980 Accuracy Assessment									
Class Value	C_1	C_2	C_3	C_4	C_5	C_6	Total	U-Accuracy	Kappa
Agriculture	39.000	0.000	0.000	0.000	2.000	2.000	43.000	0.907	0.000
Built up area	0.000	9.000	1.000	0.000	0.000	0.000	10.000	0.900	0.000
Grassland	0.000	1.000	106.000	1.000	5.000	4.000	117.000	0.906	0.000
Water bodies	0.000	0.000	0.000	10.000	0.000	0.000	10.000	1.000	0.000
Shrub land	4.000	6.000	10.000	4.000	118.000	1.000	143.000	0.825	0.000
Bare land	2.000	4.000	3.000	5.000	10.000	169.000	193.000	0.876	0.000
Total	45.000	20.000	120.000	20.000	135.000	176.000	516.000	0.000	0.000
Accuracy	0.867	0.450	0.883	0.500	0.874	0.960	0.000	0.874	0.000
Kappa	0.000	0.000	0.000	0.000	0.000	0.000	0.000	0.000	0.829

LULC 2000 Accuracy Assessment									
Class Value	C_1	C_2	C_3	C_4	C_5	C_6	Total	U_ Accuracy	Kappa
Agriculture	72.000	2.000	2.000	0.000	3.000	0.000	79.000	0.911	0.000
Built up area	3.000	25.000	2.000	0.000	0.000	0.000	31.000	0.806	0.000
Grassland	16.000	2.000	126.000	0.000	4.000	0.000	148.000	0.851	0.000
Water bodies	2.000	0.000	0.000	8.000	0.000	0.000	10.000	0.800	0.000
Shrub land	19.000	5.000	3.000	0.000	120.000	0.000	147.000	0.816	0.000
Bare land	14.000	1.000	2.000	0.000	1.000	75.000	93.000	0.806	0.000
Total	126.000	35.000	135.000	8.000	128.000	75.000	508.000	0.000	0.000
P_ Accuracy	0.571	0.714	0.933	1.000	0.938	1.000	0.000	0.839	0.000
Kappa	0.000	0.000	0.000	0.000	0.000	0.000	0.000	0.000	0.793

LULC 2010 Accuracy Assessment									
Class Value	C_1	C_2	C_3	C_4	C_5	C_6	Total	U_ Accuracy	Kappa
Agriculture	36.000	1.000	2.000	0.000	0.000	0.000	40.000	0.900	0.000
Built up area	2.000	37.000	1.000	0.000	1.000	0.000	41.000	0.902	0.000
Grassland	6.000	3.000	100.000	0.000	0.000	0.000	109.000	0.917	0.000
Water bodies	1.000	0.000	1.000	8.000	0.000	0.000	10.000	0.800	0.000
Shrub land	8.000	1.000	1.000	0.000	134.000	0.000	144.000	0.931	0.000
Bare land	7.000	5.000	2.000	0.000	0.000	151.000	165.000	0.915	0.000
Total	60.000	47.000	107.000	8.000	135.000	151.000	509.000	0.000	0.000
P_Accuracy	0.600	0.787	0.935	1.000	0.993	1.000	0.000	0.916	0.000
Kappa	0.000	0.000	0.000	0.000	0.000	0.000	0.000	0.000	0.890

LULC 2020 Accuracy Assessment									
Class Value	C_1	C_2	C_3	C_4	C_5	C_6	Total	U_ Accuracy	Kappa
Agriculture	138.000	8.000	7.000	6.000	7.000	6.000	172.000	0.802	0.000
Built up area	0.000	53.000	1.000	1.000	1.000	0.000	56.000	0.946	0.000
Grassland	3.000	3.000	91.000	1.000	1.000	2.000	101.000	0.901	0.000
Water bodies	0.000	0.000	0.000	10.000	0.000	0.000	10.000	1.000	0.000
Shrub land	1.000	1.000	1.000	0.000	64.000	0.000	67.000	0.955	0.000
Bare land	6.000	0.000	0.000	0.000	0.000	99.000	105.000	0.943	0.000
Total	148.000	65.000	100.000	18.000	73.000	107.000	511.000	0.000	0.000
P_Accuracy	0.932	0.815	0.910	0.556	0.877	0.925	0.000	0.890	0.000
Kappa	0.000	0.000	0.000	0.000	0.000	0.000	0.000	0.000	0.861

Table 6. The area coverage of LULC, percent, and rate of changes in the Study area between 1980, 2000, 2010, and 2020.

Class LULC	LULC 1980 area /km2	LULC 2000 area /km2	Land Use Dynamic Degree 1980-2000(%)	Land Use Dynamic Rate 1980-2000(%)	LULC 2010 area /km2	Land Use Dynamic Degree2000-2010(%)	Land Use Rate 2000-2010(%)	LULC 2020 area /km2	Land Use Dynamic Degree 2010-2020 (%)	Land Use Rate 2010-2020 (%)
Agriculture	636.23	1172.64	4.215.5	84.310.7	596.67	702.703.7	607.703.	2557.49	13.197.4	320.8448
Built up area	514.13	461.35	-0.513.2	-10.265.8	614.1	-5986.948	-6081.948	829.21	-5.692.5	-113.6339
Grassland	1535.09	2211.77	2.204.04	44.080.8	1619.57	3669.09368	3574.0936	1502.11	-2.953.02	-57.97228
water	273.12	22.73	-4.583.8	-91.677.6	15.96	-22.408.8	-117.4088	2.93	-5.653.7	-102.4955
Shrub land	2129.25	2193.49	0.150.8	3.017.02	2152.22	71330.84114	71235.84114	996.59	-4.930.1	-98.60099
bare land	2362.15	1387.99	-2.062.01	-41.240.3	2451.46	-5949.317	-6044.317401	1561.63	-6.312.4	-125.8363
TOT	7449.97	7449.97			7449.97			7449.97		

The agricultural land represents the predominant land use and land cover (LULC) type within the study area, accounting for 8.54% in 1980, 15.74% in 2000, 8.01% in 2010, and 34.33% in 2020 (see Table 7). The alterations in LULC have had a notable impact on the distribution of woodlands in the region. The area designated as shrubland, which constitutes the largest segment of the land use classification, has experienced a significant reduction, decreasing from 2,129.25 km² in 1980 to 996.59 km² in 2020. Conversely, the area allocated to agricultural use has increased markedly, rising from 636.23 km² in 1980 to 2,557.49 km² in 2020. This analysis reveals a substantial expansion of both agricultural and urban land, alongside a considerable decline in shrubland within the study area.

3-3 Analysis of change rate between different models

Tables 6 and 7 present the statistical data on land use dynamic changes in the study area for the years 1980, 2000, 2010, and 2020. The most significant change during the period from 1980 to 2000 occurred in bare land, which experienced a change rate of 2,362.15 km². Its transfer and loss rates were -41.2% and 2.06%, respectively. The second most rapid change rate was observed in shrubland.

Figure 4 Gain and loss areas of 1980, 2000, 2010, and 2020

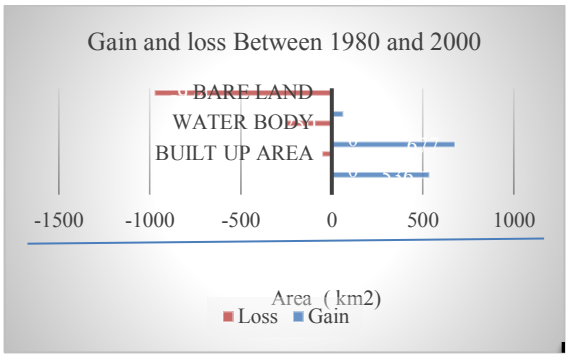

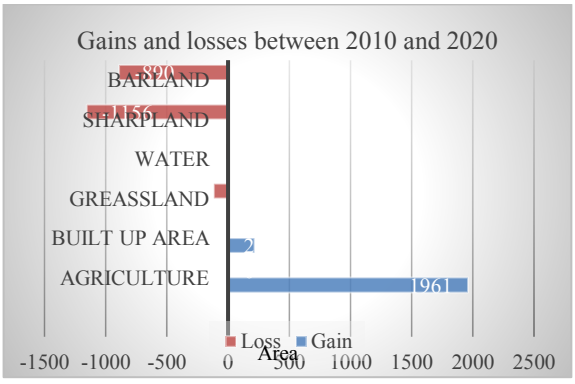

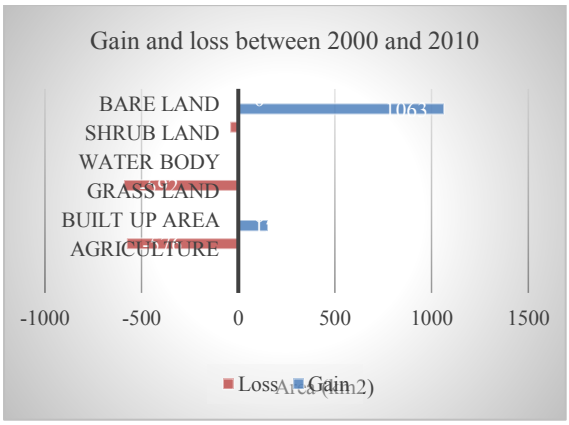

The transfer and gain rates for shrubland were not specified, and the dynamic rate was also omitted. Change rates for water and grassland were minimal, recorded at 0 km² and an unspecified value, respectively. However, their dynamic rates were the highest, although the specific values were not provided. The change rate and dynamic rate for land overall were the lowest, also lacking specific values.

3.4. Land Use and Land Cover Change Transition Matrix from 1980–2020

Transition potential modeling evaluates the likelihood of land use and land cover (LULC) changing from one class to another, depending on the suitability of the area and the presence of driving forces [98]. This modeling records the probability of each land use class transitioning into another. Future predictions of LULC changes are derived from the transition probability matrix [98]. The transition probability matrices generated by the model for LULC types during the periods 1980–2000, 2000–2010, and 2010–2020 are presented in Table 8. A spatiotemporal assessment of LULC changes between earlier and later land cover maps was conducted through cross-tabulation. This cross-tabulation helps determine the extent of change and conversions between different lands cover maps. In the cross-tabulation table shown in Table 8, the bolded frequencies along the diagonal of the transition probability matrix confirm the probability of the LULC class remaining unchanged (persistence) from the earlier to the later land cover map. In contrast, the off-diagonal frequencies indicate the likelihood of a given LULC class changing from one type to another. The change analysis is based on the differences in LULC between time 1 and time 2 [98]. The conversion of shrubland, and grassland significantly contributed to the expansion of agricultural land. The least loss of LULC categories was observed in the transition from shrubland to grassland and urban land. Between 2000 and 2010, the most significant loss occurred with the conversion of grassland to agricultural land, quantified at 2218. Before 1980 and even before 2000, the study areas were predominantly covered with shrublands and grasslands. The expansion of built-up areas has been consistently increasing at the highest rate.

Table 7 LULC of the Study area for 1980-2020

Class LULC	LULC 1980 area /km2	LULC1980 %100	LULC 2000 area /km2	LULC2000 %100	LULC 2010area /km2	LULC2010 %100	LULC 2020 area /km2	LULC2020%100
Agriculture	636.23	8.54	1172.64	15.74	596.67	8.01	2557.49	34.33
Built-up area	514.13	6.90	461.35	6.19	614.10	8.24	829.21	11.13
Grassland	1535.09	20.61	2211.77	29.69	1619.57	21.74	1502.11	20.16
water	273.12	3.67	22.73	0.31	15.96	0.21	2.93	0.04
Shrub land	2129.25	28.58	2193.49	29.44	2152.22	28.89	996.59	13.38
bare land	2362.15	31.71	1387.99	18.63	2451.46	32.91	1561.63	20.96
TOT	7449.97	100.00	7449.97	100	7449.97	100.00	7449.97	100.00
P_Accuracy	0.837		0.85		0.8375		0.7621	
U_Accuracy	0.798		0.77		0.8033		0.742	

Table (8) Land Use Land Cover Transition km2 1980 -2020

(a)

Land Use Land Cover Transition km2 1980 -2000							
Land Use Land Cover	agriculture	bar land	Built up Area	grassland	sharp land	water	Grand Total
Agriculture	139	636		9	170	5	1156
Bare land	72	346	9	408	528	4	1367
Built up Area	47	208	8	88	93	0	445
Grassland	181	1314	18	342	354	10	2218
Shrub land	154	434	7	666	925	7	2194
Water Body	0	1	0	16	5	0	22
Total	593	2939	42	1529	2075	26	7402

(b)

Land Use Land Cover Transition km2 2000 -2010							
Land Use Land Cover	Agriculture	Bare land	Built up Area	Grassland	Shrub land	water	Grand Total
Agriculture	70.76	155.14	26.18	136.44	199.59	6.33	594.43
Bare land	415.53	374.31	176.25	905.47	568.46	2.02	2442.04
Built up Area	141.58	71.18	80.99	220.05	95.24	2.7	611.73
Grassland	356.31	218.84	94.22	703.37	238.35	2.12	1613.21
Shrub land	174.92	546.42	69.02	258.12	1094.84	0.76	2144.07
Water Body	0.11	4.95	0.07	0.19	2.7	7.87	15.9
Total	1159.21	1370.84	446.73	2223.64	2199.18	21.8	7421.38

(c)

Land Use Land Cover Transition km2 2010 -2020							
Land Use Land Cover	agriculture	bar land	Built up Area	grassland	sharp land	water	Grand Total
Agriculture	443.05	29.8	48.07	19.43	53.87	0.17	594.4
Bare land	718.7	636.01	302.36	716.01	68.46	0.46	2442
Built up Area	224.7	142.39	128.21	109.12	6.73	0.57	611.73
Grassland	255.69	554.96	172.81	623.17	6.55	0.01	1613.18
Shrub land	915.8	184.98	143.68	32.63	865.61	1.36	2144.06
Water Body	15.66	0.09	0.13	0	0.01	0	15.89
Total	2573.6	1548.23	795.26	1500.36	1001.23	2.57	7421.26

3-5 Land Use Land Cover Change Prediction

Future land use and land cover (LULC) conditions in El Khuwei area were projected by analyzing historical change trends. Figure 6 and Table 9 illustrate the anticipated LULC dynamics for the years 2030 and 2050, as simulated using the Cellular Automata-Markov (CA-Markov) model. The results indicate a consistent increase in both agricultural land and built up areas in El Khuwei area compared to the reference year of 2020. Specifically, the area designated for agriculture land, which comprised 2557.49 km² (34.33%) in 2020, is expected to expand to 3314.46 km² (44.49%) in 2030 and 3845.38 km² (51.62%) in 2050 (Table 9). Moreover, the fragmented grassland areas within the study region are anticipated to experience an increase in settlement, rising from 829.21 km² (11.13%) in 2020 to 832.22 km² (11.17%) in 2030 and 802.85 km² (10.78%) in 2050 (Table 9). As depicted in Figures 6a and 6b, a significant expansion of settlements in and around El Khuwei area is predicted, with future shrubland and agricultural areas adjacent to the settlements serving as primary contributors to this growth. Conversely, the study area is expected to witness a consistent decline in shrubland, and grassland areas relative to the reference year of 2020. The projections suggest that shrubland will decrease to 686.12 km² (9.21%) and 476.04 km² (6.39%) in 2030 and 2050, respectively; and grassland will diminish to 1242.77 km² (16.68%) and 1111.49 km² (14.92%) in the same years. Under this scenario, it is anticipated that the shrubland areas in the study area will be converted to settlement and cultivated land. (Figure 6a, b).

Figure 5. Distribution of the LULC class that transitioned between 1980 –2020

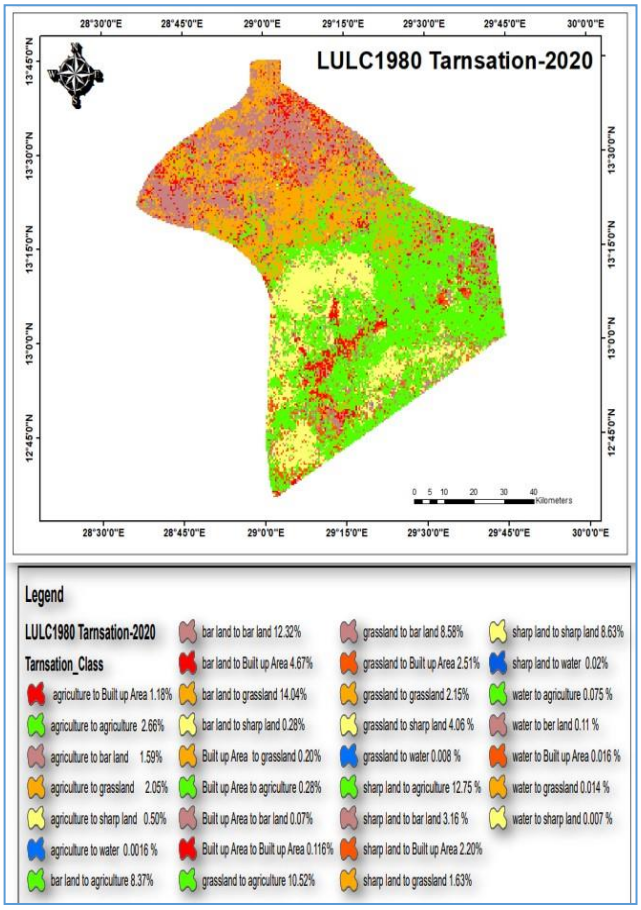

Figure 6. Potential distribution of LULC types of the study area in 2030, 2050.

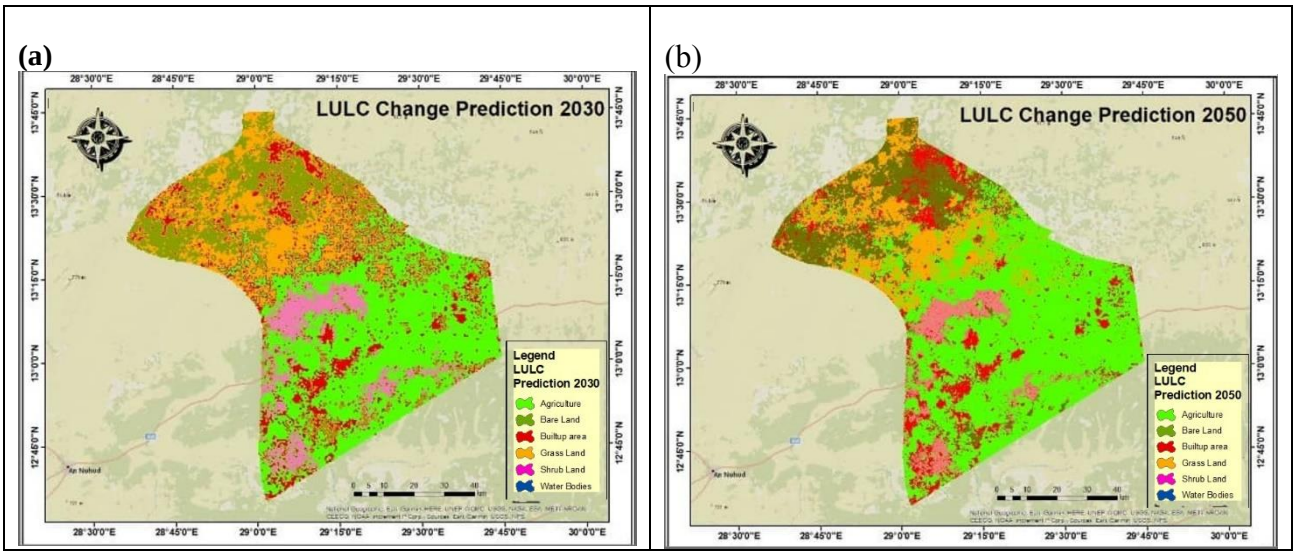

A significant change was identified in the land use and land cover (LULC) analysis results between 1980 and 2050.

Agricultural land is projected to become the predominant LULC type. The analysis indicates that the area designated as agricultural land is expected to increase from 34.33%% in 2020 to 44.49% in 2030, and subsequently to 51.62% in 2050. This increase is primarily attributed to the conversion of shrubland, and portions of grassland into agricultural use.

Notably, agricultural land experienced substantial growth from 1980 to 2030, followed by a more gradual increase from 2030 to 2050 (as illustrated in the accompanying figure and table). Additionally, a continuous increase in urban areas was observed during the period from 2020 to 2030. The total area covered by settlements was recorded at 6.90% in 1980, with projections indicating an increase to 11.17% by 2030 and 10.78% by 2050. The graphical representation of the area covered by six LULC classes for the years 1980, 2000, 2010, and 2020, as well as the projected years 2030 and 2050, is presented in Figure 6.

Table (9) LULC Dynamic Degree, Dynamic Rate.

Class LULC	LULC 2020 area /km2	Land Use Dynamic Degree 2010-2020 (%)	Land Use Rate 2010-2020 (%)	LULC Prediction 2030 area /km2	Land Use Dynamic Degree 2020-2030 (%)		LULC Prediction 2050 area /km2	Land Use Dynamic Degree 2030 - 2050(%)	Land Use Rate 2030 -2050(%)
Agriculture	2557.49	13.19749858	320.8448793	3314.46	1250.715233	933.041265	3845.38	10.37272394	312.1339692
Built up area	829.21	-5.692514745	-113.6339534	832.22	-735.9774653	-832.3691338	802.85	-10.45431102	-196.4536006
Grass land	1502.11	-2.953023102	-57.97228236	1242.77	-2109.233454	-2243.731365	1111.49	-7.634819769	-149.5375702
Water Body	2.93	-5.65376035	-102.4955535	27.75	-29.54118877	-127.0743452	89.24	-20.10433461	-170.2266062
Shrub land	996.59	-4.93014312	-98.60099918	686.12	-700.8418684	-795.8550174	476.04	-8.396201208	-159.8149147
Bare land	1561.63	-6.312444685	-125.8363335	1346.65	-1071.662812	-1170.159916	1124.97	-10.2487125	-196.1381419
TOT	7449.97			7449.97			7449.97		

4. Conclusions

This study analyzed historical land use and land cover change (LULCC) from 1980 to 2020 as well as projected land use and land cover (LULC) for 2030 and 2050 through the application of the AC-MC Chain model in the semi-arid region of Kordofan, Sudan. The main findings indicate that significant spatial and temporal changes have occurred. From 1980 to 2020, there was a notable increase in agricultural areas and settlements, alongside a decrease in bare ground within the study area. Projections for LULC in 2030 and 2050 suggest that the expansion of agricultural areas and settlements will have environmental implications. The analysis of LULCC indicates an increase in settlements and agricultural areas, as well as a decrease in bare ground between 1980 and 2000. Between 2000 and 2010, settlements continued to rise; however, there was a decline in shrubland, grass areas, and bare ground. By 2050, based on trends observed from 2000 to 2010 and 2020, land use changes are expected to progress in a manner that is incompatible with maintaining a balanced environment. The analysis of surface state dynamics revealed that population growth and evolving anthropogenic (socioeconomic) activities were the primary drivers of LULC changes. These changes in LULC present both positive and negative outcomes. El Khuwei area has experienced a trend toward increased population and deforestation, accompanied by the adoption of sustainable land management practices, which can enhance water and land conservation efforts.

Acknowledgments

The authors are grateful to the Faculty of Geographical and Environmental Sciences, University of Khartoum for providing technical support for this study.

Conflicts of Interest

The authors declare no conflict of interest.

References:-

[1] Abd El-Hamid, H.T., Caiyong, W., Hafiz, M.A. *et al.* **(2020)**. Effects of land use/land cover and climatic change on the ecosystem of North Ningxia, China. *Arab J Geosci* **13**, 1099. https://doi.org/10.1007/s12517-020-06047-6

[2] Abera, T. A., Heiskanen, J., Pellikka, P. K. E., Adhikari, H. & Maeda, E. E. **(2020)**. Climatic impacts of bushland to cropland conversion in Eastern Africa. Sci.Total Environ. 717, 137255.

[3] Abere T., E. Adgo, S. Afework, **(2020).** Trends 2020 of land use/cover change in Kecha-Laguna paired micro watersheds, Northwestern Ethiopia Cogent Environmental Science, 6 (1) Article 1801219 Google Scholar

[4] ADAM, H. E., OSMAN, Y. M., ELAMIN, H. M. A., & ELTAHIR, M. E. S. (2022). ASSESSMENT OF LAND USE AND LAND COVER CHANGES IN ERRAHAD LOCALITY, SUDAN, USING REMOTE SENSING AND GIS. JOURNAL OF GLOBAL AGRICULTURE AND ECOLOGY, 14(4), 71–78. HTTPS://DOI.ORG/10.56557/JOGAE/2022/V14I47876

[5] Ahmed, H., Kheiry, M., & Yasin, E. **(2023)**. Land-Use Land-Cover Change Detection Using Geospatial Techniques in Zalingei, Central Darfur, Sudan. *Journal of Information Systems and Informatics*, *5*(4), 1676-1690. https://doi.org/10.51519/journalisi.v5i4.624

[6] Ahmed, M., Shuai, J., Ali, H. **(2023).** The effects of climate change on food production in India: Evidence from the ARDL model. *Environment, Development and Sustainability*https://doi.org/10.1007/s10668-023-03209-w

[7] Aliani, H., Malmir, M., Sourodi, M., & Kafaky, S. B. **(2019).** Change Detection and Prediction of Urban Land Use Changes by CA-Markov Model (Case Study: Talesh County). Environmental Earth Sciences, 78, Article No. 546.https://doi.org/10.1007/s12665-019-8557-9

[8] Amini, S., Saber, M., Rabiei Dastjerdi, H., & Homayouni, S. **(2022)**. Urban land use and land cover change analysis using random forest classification of Landsat time series. *Remote Sensing*, *14*(11), 1–23. https://doi.org/10.3390/ rs14112654 (Open in a new window)Google Scholar

[9] Andrieu, J. **(2018)**. Land cover changes on the West-African coastline from the Saloum Delta (Senegal) to Rio Geba (Guinea-Bissau) between 1979 and 2015 land cover changes on the West-African coastline from the Saloum Delta. *European Journal of Remote Sensing*, *51*(1), 314–325. https://doi.org/10.1080/22797254.2018.1432295

[10] Aneseyee. A.B, E. Elias, T. Soromessa, G.L. Feyisa **(2020).** Land use/land cover change effect on soil erosion and sediment delivery in the Winike watershed, Omo Gibe Basin, Ethiopia. Science of the Total Environment, 728 Article 138776

[11] Armin, M., Majidian, M. & Kheybari, V.G. **(2020)**. Land Use/Land Cover Change Detection and Prediction in the Yasouj City Suburbs in Kohgiluyeh Va Boyerahmad Province in Iran. *Arid Ecosyst* **10**, 203–210. https://doi.org/10.1134/S207909612003012

[12] Asibey, M.O.; Agyeman, K.O.; Amponsah, O.; Ansah, T. (**2019)**. Patterns of land use, crop and forest cover change in the Ashanti region, Ghana. J. Sustain. For. 1–26. [Google Scholar] [CrossRef]

[13] Barnieh, B., Jia, L., Menenti, M., Zhou, J., & Zeng, Y. **(2020)**. Mapping Land Use Land Cover Transitions at Different Spatiotemporal Scales in West Africa. *Sustainability*, *12*(20), 8565. https://doi.org/10.3390/su12208565

[14] Basheer, S., X. Wang, A. A. Farooque, R. Ali Nawaz, K. Liu, T. Adekanmbi, and S. Liu. **(2022).** "Comparison of Land Use Land Cover Classifiers Using Different Satellite Imagery and Machine Learning Techniques." *Remote Sensing* 14(open in a new window) (19(open in a new window)): 4978. https://doi.org/10.3390/rs14194978.(Open in a new window)Web of Science ®(Open in a new window)Google Scholar

[15] Bashir, O., Bangroo, S. A., Guo, W., Meraj, G., T. Ayele, G., Naikoo, N. B., Shafai, S., Singh, P., Muslim, M., Taddese, H., Gani, I., & Rahman, S. U. **(2022)**. Simulating Spatiotemporal Changes in Land Use and Land Cover of the North-Western Himalayan Region Using Markov Chain Analysis. *Land*, *11*(12), 2276. https://doi.org/10.3390/land11122276

[16] Berihun, M.L.; Tsunekawa, A.; Haregeweyn, N.; Meshesha, D.T.; Adgo, E.; Tsubo, M.; Masunaga, T.; Fenta, A.A.; Sultan, D.;Yibeltal, M.(**2019)**. Exploring land use/land cover changes, drivers, and their implications in contrasting agro-ecological environments of Ethiopia. Land Use Policy 87, 104052. [CrossRef]

[17] Brandt, M.; Mbow, C.; Diouf, A.A.; Verger, A.; Samimi, C.; Fensholt, R. (**2014)**. Ground and satellite-based evidence of the biophysical mechanisms behind the greening Sahel. Glob. Chang. Biol. 21, 1610–1620. [**Google Scholar**] [**CrossRef**] [**Green Version**]

[18] Buğday E, Buğday SE. **(2019).** Modeling and simulating land use/cover change using artificial neural network from remotely sensing data. Cerne. 25(2):246–254. (Open in a new window)Web of Science ®(Open in a new window)Google Scholar

[19] Chang, Y., Hou, K., Li, X., Zhang, Y., & Chen, P. **(2018).** Review of land use and land cover change research progress. *IOP Conference Series: Earth and Environmental Science*, *113*(1). https://doi.org/10.1088/1755-1315/113/1/012087

[20] Chen, Y., Yuan, H., Yang, Y., & Sun, R. (2020). Sub-daily soil moisture estimate using dynamic Bayesian model averaging. *Journal of Hydrology, 590*, 125445.

[21] Cui, G.; Lv, Z.; Li, G.; Benediktsson, A.J.; Lu, Y. (**2018)**. Refining Land Cover Classification Maps Based on Dual-Adaptive Majority Voting Strategy for Very High-Resolution Remote Sensing Images. Remote Sens. 10, 1238. [Google Scholar] [CrossRef] [Green Version]

[22] Deng, Z., and B. Quan. **(2022).** "Intensity Characteristics and Multi-Scenario Projection of Land Use and Land Cover Change in Hengyang, China." *International Journal of Environmental Research and Public Health* 19(14): 8491. https://doi.org/10.3390/ijerph19148491. (Open in a new window)PubMed (Open in a new window)Web of Science ®(Open in a new window)Google Scholar

[23] Dey, N.N., Rakib, A.A., Kafy, A.-, & Raikwar, V. **(2021)**. Geospatial modelling of changes in land use/land cover dynamics using Multi-layer perception Markov chain model in Rajshahi City, Bangladesh. ENVIRON. CHALL, 4, 100148. [GOOGLE SCHOLAR] [CROSSREF]

[24] Dolui, S., and S. Sarkar. **(2023)**. "Modelling Landuse Dynamics of Ecologically Sensitive Peri-Urban Space by Incorporating an ANN Cellular Automata-Markov Model for Siliguri Urban

Agglomeration, India." *Modeling Earth Systems and Environment* 10(open in a new window) (1(open in a new window)): 167–199. https://doi.org/10.1007/s40808-023-01771-w.(Open in a new window)Google Scholar

[25] Elhaja ME, Csaplovics E, Abdelkareem OE, Adam HE, Khalifa AE, Ibrahim KA, Eltahir ME **(2017)**. Land use land cover change detection in White Nile State, Sudan using remote sensing and GIS techniques. International Journal of Environmental Monitoring and Protection. 4(3):14–19.Google Scholar

[26] FAO, **(2015).** Climate Change and Food Security: Risks and Responses; Food & Agriculture Organization: Rome, Italy.

[27] FAO. Watershed Management in Action: Lessons Learned from FAO Field Projects; Food & Agriculture Organization: Rome, Italy, pp. 5–6.

[28] FAO **(2020)**. Global Forest Resources Assessment 2020 (FRA 2020). No 163. Rome, Italy. Forestry Paper. GOOGLE SCHOLAR

[29] Fathizad, H.; Rostami, N.; Faramarzi, M. (**2015)**. Detection and prediction of land cover changes using Markov chain model in semi-arid rangeland in western Iran. Environ. Monit. Assess. 187, 1–12. [CrossRef

[30] Foody GM. 2020. Explaining the unsuitability of the kappa coefficient in the assessment and comparison of the accuracy of thematic maps obtained by image classification. Remote Sens Environ. 239(open in a new window):111630. doi: 10.1016/j.rse.2019.111630. (Open in a new window)Web of Science ®(Open in a new window)Google Scholar

[31] Gaur, S., & Singh, R. (2023). A Comprehensive Review on Land Use/Land Cover (LULC) Change Modeling for Urban Development: Current Status and Future Prospects. *Sustainability*, *15*(2), 903. https://doi.org/10.3390/su15020903

[32] Gaur, S.; Singh, B.; Bandyopadhyay, A.; Stisen, S.; Singh, R. (**2022).** Spatial pattern-based performance evaluation and uncertainty analysis of a distributed hydrological model. Hydrol. Processes, 36, e14586. [CrossRef]

[33] Geist, H.J.; Lambin, E.F. Dynamic Causal Patterns of Desertification. BioScience **2004**, 54, 817–829. [CrossRef]

[34] Gidey, E., Dikinya, O., Sebego, R., Segosebe, E., & Zenebe, A. **(2017)**. Cellular automata and Markov Chain (CA_Markov) model-based predictions of future land use and land cover scenarios (2015–2033) in Raya, northern Ethiopia. *Modeling Earth Systems and Environment*, *3*, 1245-1262.

[35] Govender T, Dube T, Shoko C. **(2022).** Remote sensing of land use land cover change, and climate variability on hydrological processes in Sub-Saharan Africa: key scientific strides and challenges. Geocarto Int. 37(open in a new window)(25(open in a new window)):10925–10949. doi: 10.1080/10106049.2022.2043451. Web of Science ® Google Scholar

[36] Govender, T., Dube, T., & Shoko, C. **(2022).** Remote sensing of land use land cover change and climate variability on hydrological processes in Sub-Saharan Africa: key scientific strides and challenges. Geocarto International, 37(25), 10925–10949. https://doi.org/10.1080/10106049.2022.2043451

[37] Guptha, G.C., Swain, S., Al-Ansari, N., Taloor, A.K., & Dayal, D. **(2021).** Evaluation of an urban drainage system and its resilience using remote sensing and GIS. *Remote Sensing Applications: Society and Environment*.

[38] Hamad, R.; Balzter, H.; Kolo, K. (**2018).** Predicting land use/land cover changes using a CA-Markov model under two different scenarios. Sustainability, 10, 3421. [CrossRef]

[39] Harrison, M.N. and Jackson, J.K. (1958) Ecological Classification of the Vegetation of the Sudan. Forest Bulletin No. 2, Forest Department, Ministry of Agriculture, Khartoum, Sudan.

[40] Hasan, S.; Shi, W.; Zhu, X.; Abbas, S.; Khan, H.U.A.(**2020).** Future simulation of land use changes in rapidly urbanizing South China based on land change modeler and remote sensing data. Sustainability 12, 4350. [CrossRef]

[41] Herrmann, S.M., Brandt, M., Rasmussen, K. *et al.* **(2020)**. Accelerating land cover change in West Africa over four decades as population pressure

increased. *Commun Earth Environ* **1**, 53 https://doi.org/10.1038/s43247-020-00053-y

[42] Huang, W.; Luan, Q.; Jiang, Q.; Liu, J.; Liu, H. (**2008**). Detection and prediction of land use change in Beijing based on remote sensing and GIS. The international archives of photogrammetry. Remote Sens. Spat. Inf. Sci. 37, 6b.

[43] Hyandye, C. (**2015**). GIS and logit regression model applications in land use and land cover change and distribution in Usangu catchment. Am. J. Remote Sens. 3, 6–16.

[44] Iqbal, M., & Sajjad, H. (**2014**). Watershed prioritization using morphometric and land use/land cover parameters of Dudhganga catchment, Kashmir Valley, India, using spatial technology. *Journal of Geophysics & Remote Sensing*, 03(01). https://doi.org/10.4172/2169-0049.1000115

[45] Iqbal, M., Sajjad, H., B, F. A., & Ahm, I. **(2013).** Monitoring of water quality parameters in upper and lower reaches of Dudhganga catchment, India. In *Perspectives in water pollution*. InTechhttps://doi.org/10.5772/52846

[46] Jia, W., Gu, X., Mi, X., Yang, J., Zang, W., Liu, P., Yan, J., Zhu, H., Zhang, X., & Zhang, Z. **(2022).** Multi-Scale Spatiotemporal Pattern Analysis and Simulation (MSPAS) Model with Driving Factors for Land Cover Change and Sustainable Development Goals: A Case Study of Nepal. *Remote Sensing*, *14*(24), 6295. https://doi.org/10.3390/rs14246295

[47] Jin, S., Yang, L., Danielson, P., Homer, C., Fry, J., Xian, G., **(2013)**. A comprehensive change detection method for updating the national land cover database to circa 2011. Remote Sens. Environ. 132, 159–175.

[48] Jining, Y.;Wang, L.; Song,W.; Chen, Y.; Chen, X.; Deng, Z**.(2019),** A time-series classification approach based on change detection for rapid land cover mapping. ISPRS J. Photogramm. Remote Sens. 158, 249–262. [CrossRef]

[49] Karki, S., Thandar, A.M., Uddin, K. et al **(2018)**, Impact of land use land cover change on ecosystem services: a comparative analysis on observed data and people's perception in Inle Lake, Myanmar. Environ Syst Res 7, 25. https://doi.org/10.1186/s40068-018-0128-7

[50] Kumar, S.; Radhakrishnan, N.; Mathew, S. (**2014).** Land use change modelling using a Markov model and remote sensing. Geomat. Nat.Hazards Risk, 5, 145–156. [CrossRef]

[51] Lambin, E.F., Geist, H.J. and Lepers, E. **(2003)** Dynamics of Land-Use and Land-Cover Change in Tropical Regions. Annual Review of Environment and Resources, 28, 205-241. http://dx.doi.org/10.1146/annurev.energy.28.050302.105459

[52] Leta, M.K.; Demissie, T.A.; Tranckner, J. (**2021**), Modeling and prediction of land use land cover change dynamics based on land change modeler (LCM) in Nashe watershed, Upper Blue Nile basin, Ethiopia. Sustainability 13, 3740. [CrossRef]

[53] Li, X.; Chen, G.; Liu, X.; Liang, X.; Wang, S.; Chen, Y.; Pei, F.; Xu, X. (**2017).** A New Global Land-Use and Land-Cover Change Product at a 1-km Resolution for 2010 to 2100 Based on Human-Environment Interactions. Ann. Am. Assoc. Geogr. 107, 1040–1059. [CrossRef]

[54] Liping C, Yujun S, Saeed S **(2018)** Monitoring and predicting land use and land cover changes using remote sensing and GIS techniques—a case study of a hilly area, Jiangle. China. PLoS One 13(7):e0200493 **PubMed Google Scholar**

[55] Lu, D., Mausel, P., Brondizio, E., Moran, E. **(2004)**. Change detection techniques. Int. J. Remote Sens. 25 (12), 2365–2401.

[56] Lv, Z., Liu, T., Wan, Y., Benediktsson, J.A., Zhang, X. **(2018)**. Post-processing approach for refining raw land cover change detection of very high-resolution remote sensing images. Remote Sens. 10, 472.

[57] Mas, J. F., & Flores, J. J. **(2008**). The application of artificial neural networks to the analysis of remotely sensed data. *International Journal of Remote Sensing*, *29*(3), 617–663. https://doi.org/10.1080/01431160701352154

[58] Mas, J., Kolb, M., Paegelow, M., Camacho, M. T., Houet, T., Mas, J., Kolb, M., Paegelow, M., Teresa, M., Olmedo, C., & Houet, T. **(2014)**. Inductive pattern-based land use/ cover change models: A comparison of four software packages. In

Environmental Modelling & Software (pp. 94–111). Elsevier. https://doi.org/10.1016/j.envsoft.2013. 09.010. hal-01187569HAL

[59] Mas, J.F.; Pérez-Vega, A.; Clarke, K.C. (**2012**). Assessing simulated land use/cover maps using similarity and fragmentation indices. Ecol. Complex. 11, 38–45. [CrossRef]

[60] Mishra VN, Rai PK, Kumar P, Prasad R. **(2016)** Evaluation of land use/land cover classification accuracy using multi-resolution remote sensing images. Forum geografic. XV (1):45±53. https://doi.org/10.5775/

[61] Mishra, V. N., Rai, P. K., Prasad, R., Punia, M., & Nistor, M. M. **(2018)**. Prediction of spatio-temporal land use/land cover dynamics in rapidly developing Varanasi district of Uttar Pradesh, India, using geospatial approach: A comparison of hybrid models. *Applied Geomatics*, *10*(3), 257–276. https://doi.org/10.1007/ s12518-018-0223-5

[62] Mishra, V., Rai, P., & Mohan, K. **(2014)**. Prediction of land use changes based on land change modeler (LCM) using remote sensing: A case study of Muzaffarpur (Bihar), India. *Journal of the Geographical Institute Jovan Cvijic, SASA*, *64*(1), 111–127. https://doi.org/10.2298/ ijgi1401111m

[63] Motlagh, Z.K., Lotfi, A., Pourmanafi, S. *et al.* **(2020).**Spatial modeling of land-use change in a rapidly urbanizing landscape in central Iran: integration of remote sensing, CA-Markov, and landscape metrics. *Environ Monit Assess* **192**, 695 https://doi.org/10.1007/s10661-020-08647-x

[64] Munthali, M. G., Mustak, S., Adeola, A., Botai, J., Singh, S. K., & Davis, N. **(2020).** Modelling land use and land cover dynamics of Dedza district of Malawi using hybrid cellular automata and Markov model. *Remote Sensing Applications: Society and Environment, 17*, 100276. **Google Scholar**

[65] Mustafa EK, Liu G, Abd El-Hamid HT, Kaloop MR. **(2019)**. Simulation of land use dynamics and impact on land surface temperature using satellite data. GeoJournal. DOI: https://doi.org/https://doi.org/10.1007/ s10708-019-10115-0(open in a new window). Google Scholar

[66] Nadoushan, M.; Soffianian, A.; Alebrahim, A. (**2015).** Modeling Land Use/Cover Changes by the Combination of Markov Chain and Cellular Automata Markov (CA-Markov) Models. J. Earth Environ. Health Sci. 1, 16. [CrossRef]

[67] Nasiri, V., Deljouei, A., Moradi, F., Sadeghi, S. M. M., & Borz, S. A. **(2022)**. Land use and land cover mapping using Sentinel-2, Landsat-8 satellite images, and Google Earth Engine: a comparison of two composition methods. *Remote Sensing*, *14*(9), 1977. https://doi.org/10.3390/ rs14091977

[68] Nath, B.; Wang, Z.; Ge, Y.; Islam, K.; Singh, R.P.; Niu, Z. (**2020).** Land Use and Land Cover Change Modeling and Future Potential Landscape Risk Assessment Using Markov-CA Model and Analytical Hierarchy Process. ISPRS Int. J. Geo-Inf. 9, 134. [**Google Scholar**] [**CrossRef**] [**Green Version**]

[69] Pereira, C. O., Escanilla-Minchel, R., González, A. C., Alcayaga, H., Aguayo, M., Arias, M. A., & Flores, A. N. **(2022).** Assessment of Future Land Use/Land Cover Scenarios on the Hydrology of a Coastal Basin in South-Central Chile. *Sustainability*, *14*(24), 16363. https://doi.org/10.3390/su142416363

[70] Ren, Y.; Lü, Y.; Comber, A.; Fu, B.; Harris, P.; Wu, L. (**2019**). Spatially explicit simulation of land use/land cover changes: Current coverage and future prospects. Earth-Sci. Rev. 190, 398–415. [CrossRef]

[71] Sahana, M., Rihan, M., Deb, S., Patel, P. P., Ahmad, W. S., & Imdad, K. **(2020)**. Detecting the facets of anthropogenic interventions on the paleochannels of Saraswati and Jamuna. In Anthropogeomorphology of Bhagirathi-Hooghly river system in India (pp. 469–489). CRC Press.

[72] Sankarrao L, Ghose DK, Rathinsamy M **(2021)** Predicting land-use change: intercomparison of different hybrid machine learning models. Environ Model Softw 145:105207. https://doi.org/10.1016/j.envsoft.2021.105207 **Google Scholar**

[73] Sedano, F., Molini, V., & Azad, M. A. K. **(2019)**. A Mapping Framework to Characterize Land Use in the Sudan-Sahel Region from Dense Stacks of Landsat

Data. *Remote Sensing*, *11*(6), 648. https://doi.org/10.3390/rs11060648

[74] Sekertekin, A., Marangoz, A.M., Akcin, H., **(2017)**. Pixel-based classification analysis of land use land cover using Sentinel-2 and Landsat-8 data. Int. Arch.Photogrammetry Remote Sens. Spatial Information Sci. XLII-4/W6, 91–93.

[75] Shelestov, A., Lavreniuk, M., Kussul, N., Novikov, A., & Skakun, S. **(2017)**. Exploring Google Earth Engine platform for big data processing: Classification of multi-temporal satellite imagery for crop mapping. *Frontiers in Earth Science*, *5*(February), 1–10. https:// doi.org/10.3389/feart.2017.00017 Silva, L. P. E., Xavier, A. P. C., da

[76] Shi, G., Jiang, N., & Yao, L. **(2018)**. Land Use and Cover Change during the Rapid Economic Growth Period from 1990 to 2010: A Case Study of Shanghai. *Sustainability*, *10*(2), 426. https://doi.org/10.3390/su10020426

[77] Silva, R. M., & Santos, C. A. G. **(2020)**. Modeling land cover change based on an artificial neural network for a semiarid river basin in northeastern Brazil. *Global Ecology and Conservation*, *21*, e00811. https://doi.org/10.1016/j. gecco.2019.e00811

[78] Singh, S.K.; Mustak, S.; Srivastava, P.K.; Szabó, S.; Islam, T. (**2015**). Predicting spatial and decadal LULC changes through cellular automata Markov chain models using earth observation datasets and geo-information. Environ. Process. 2, 61–78. [CrossRef]

[79] Singh, V. G., Singh, S. K., Kumar, N., & Singh, R. P. **(2022).** Simulation of land use/land cover change at a basin scale using satellite data and Markov chain model. *Geocarto International*, *37*(26), 11339–11364. https://doi.org/10. 1080/10106049.2022.2052976

[80] Tadese, Teshome, Soromessa, Tesefaye, Bekele. **(2021)**. Analysis of the Current and Future Prediction of Land Use/Land Cover Change Using Remote Sensing and the CA-Markov Model in Majang Forest Biosphere Reserves of Gambella, Southwestern Ethiopia.. The Scientific World Journal, 2021:6685045-. doi: 10.1155/2021/6685045

[81] Thornthwaite **1948**, "Classification of Climates | Climatology | Geography". *Geography Notes*. 11 March 2017. Retrieved 5 September 2021

[82] Tong, S.T.Y.; Sun, Y.; Ranatunga, T.; He, J.; Yang, Y.J. (**2012**). Predicting plausible impacts of sets of climate and land use change scenarios on water resources. Appl. Geogr. 32, 477–489. [CrossRef]

[83] Tong, X. et al. **(2020).** The forgotten land use class: mapping of fallow fields across the Sahel using Sentinel-2. Remote Sens. Environ. 239, 111598

[84] Traore, S. S., Dembele, S., Dembele, D., Diakite, N., & Diakite, C. H. **(2022)**. Dynamique de l'occupation du sol et trajectoire du couvert végétal autour de trois sites miniers du Sud Mali entre 1988 et 2019. *Physio-Géo*, 17(open in a new window)(Volume 17(open in a new window)), 151–166. https://doi.org/10.4000/physio-geo.14565

[85] United Nations, Department of Economic and Social Affairs, Population Division. World Population Prospects: The **2019** Revision (custom data). (Acquired via website).

[86] Vu, T.T.; Shen, Y. (**2021).** Land-use and land-cover changes in Dong Trieu district, Vietnam, during past two decades and their driving forces. Land, 10, 798. [CrossRef]

[87] Wang, P.; Huang, C.; Brown de Colstoun, E.C.; Tilton, J.C.; Tan, B., (**2017**). Global Human Built-up and Settlement Extent (HBASE) Dataset from Landsat; NASA Socioeconomic Data and Applications Center (SEDAC): Palisades, NY, USA. [Google Scholar] [CrossRef]

[88] Wang, S.Q.; Zheng, X.Q.; Zang, X.B. (**2021).** Accuracy assessments of land use change simulation based on Markov-cellular automata model. Procedia Environ. Sci. 13, 1238–1245. [CrossRef]

[89] Wnek, A.; Kudas, D.; Stych, P. (**2021**). National-level land-use changes in functional urban areas in Poland, Slovakia, and Czechia. Land 10, 39. [CrossRef]

[90] Wu, T., Luo, J., Fang, J., Ma, J., Song, X. **(2018)**. Unsupervised object-based change detection via a Weibull mixture model-based binarization for high-resolution remote sensing images. IEEE Geosci. Remote Sens. Lett. 15, 63–67.

[91] Xiong, J., Thenkabail, P.S., Tilton, J.C., Gumma, M.K., Teluguntla, P.G., Oliphant, A.J., Congalton, R.G., Yadav, K.,

& Gorelick, N. **(2017**). Nominal 30-m Cropland Extent Map of Continental Africa by Integrating Pixel-Based and Object-Based Algorithms Using Sentinel-2 and Landsat-8 Data on Google Earth Engine. *Remote. Sens., 9*, 1065.

[92] Yang, C.B., He, X.Y., Yan, F.Q., Yu, L.X., Bu, K., Yang, J.C., Chang, L.P., Zhang, S.W., **(2017**). Mapping the influence of land use/land cover changes on the urban heat island effect: a case study of Changchun, China. Sustainability 9, 312.

[93] Yang, D., Wang, X., Zhang, Z., & Nawaz, Z. **(2021)**. Testing accuracy of land cover classification algorithms in the Qilian Mountains based on the GEE cloud platform. *Remote Sensing*, *13*(24). https://doi.org/10.3390/rs13245064.

[94] Yang, L., Driscol, J., Sarigai, S., Wu, Q., Chen, H., & Lippitt, C. D. **(2022).** Google Earth Engine and Artificial Intelligence (AI): A Comprehensive Review. *Remote Sensing*, *14*(14), 3253. *14*(14). https://doi.org/10.3390/rs14143253.

[95] Yang, X.; Zheng, X.-Q.; Lv, L.-N. (**2012**). Spatiotemporal model of land use change based on ant colony optimization, Markov chain, and cellular automata. Ecol. Model. 233, 11–19. [CrossRef]

[96] Yu, H., Joshi, P.K., Das, K.K., Chauniyal, D.D., Melick, D.R., Yang, X., Xu, J., **(2007)**. Land use/cover change and environmental vulnerability analysis in Birahi Ganga sub-watershed of the Garhwal Himalaya, India. Tropical Ecol. 48 (2), 241.

[97] Yuan, F., Sawaya, K.E., Loeffelholz, B., Bauer, M.E. **(2005)**. Land cover classification and change analysis of the Twin Cities (Minnesota) Metropolitan Area by multitemporal Landsat remote sensing. Remote Sens. Environ. 98, 317–328.

[98] Zhang, P., Lv, Z., Shi, W. **(2014)**. Local spectrum-trend similarity approach for detecting land-cover change by using Spot-5 satellite images. IEEE Geosci. Remote Sens. Lett. 11, 738–742.

[99] Zhao, Y.; Feng, D.; Yu, L.;Wang, X.; Chen, Y.; Bai, Y.; Hernández, H.J.; Galleguillos, M.; Estades, C.; Biging, G.S.; et al. (**2016**). Detailed dynamic land cover mapping of Chile: Accuracy improvement by integrating multi-temporal data. Remote Sens. Environ. 183, 170–185. [CrossRef]

[100] Zhu, Z., Woodcock, C.E. **(2014)**. Continuous change detection and classification of land cover using all available Landsat data. Remote Sens. Environ. 144, 152–171.